Mathematical and Computer Modelling 58 (2013) 288–299

Contents lists available at SciVerse ScienceDirect

Mathematical and Computer Modelling

journal homepage: www.elsevier.com/locate/mcm

Optical TCAD on the Net: A tight-binding study of inter-band light transitions in self-assembled InAs/GaAs quantum dot photodetectors

Hoon Ryu [a,*], Dukyun Nam [a], Bu-Young Ahn [a], JongSuk Ruth Lee [a], Kumwon Cho [a], Sunhee Lee [b], Gerhard Klimeck [c], Mincheol Shin [d,*]

[a] *Supercomputing Center, Korea Institute of Science and Technology Information, Daejeon 305-806, Republic of Korea*

[b] *Samsung Advanced Institute of Technology, Yongin, Gyeonggi-do 446-712, Republic of Korea*

[c] *Network for Computational Nanotechnology, Purdue University, West Lafayette, IN 47907, USA*

[d] *Department of Electrical Engineering, Korea Institute of Advanced Science and Technology, Daejeon 305-701, Republic of Korea*

ARTICLE INFO

Keywords:
Optoelectronics
Tight-binding
Atomistic modeling
III–V photodetector
Parallel computing
Science gateway

ABSTRACT

A new capability of our well-known NEMO 3-D simulator (Ref. Klimeck et al., 2007 [10]) is introduced by carefully investigating the utility of III–V semiconductor quantum dots as infrared photodetectors at a wavelength of 1.2–1.5 μm. We not only present a detailed description of the simulation methodology coupled to the atomistic $sp^3d^5s^*$ tight-binding band model, but also validate the suggested methodology with a focus on a proof of principle on small GaAs quantum dots (QDs). Then, we move the simulation scope to optical properties of realistically sized dome-shaped InAs/GaAs QDs that are grown by self-assembly and typically contain a few million atoms. Performing numerical experiments with a variation in QD size, we not only show that the strength of ground state inter-band light transitions can be optimized via QD size-engineering, but also find that the hole ground state wavefunction serves as a control factor of transition strengths. Finally, we briefly introduce the web-based cyber infrastructure that is developed as a government-funded project to support online education and research via TCAD simulations. This work not only serves as a useful guideline to experimentalists for potential device designs and other modelers for the self-development of optical TCAD, but also provides a good chance to learn about the science gateway project ongoing in the Republic of Korea.

1. Introduction

Quantum dots and optoelectronics. III–V compound semiconductor quantum dots (QDs) have gained scientific attention due to their potential utility as optoelectronic devices such as laser devices [1,2], photodetectors [3], and optical communication devices [4]. Especially, GaAs-based optical devices have been of great interest since they can be used for optical-fiber-based communication systems at infrared wavelengths. Indeed, there has been a huge amount of effort among several experiments to achieve polarization insensitive optical emissions at wavelengths longer than 1.2 μm by embedding InAs QDs in $In_xGa_{1-x}As$ strain reducing capping layers [5], by controlling the growth conditions of the bilayer QD stacks [6], and by adding dilute impurities such as nitride forming InGaNAs alloy [7].

Need for atomistic simulations. Device downscaling has been the leading paradigm of the semiconductor industry ever since the invention of the first transistor in 1947 [8], where the device size these days has already reached a few tens of nanometers. In such a *nanoscale* regime, two conceptual changes are required in the device modeling methodology.

* Corresponding authors.
E-mail addresses: elec1020@gmail.com (H. Ryu), mshin@kaist.ac.kr (M. Shin).

0895-7177/$ – see front matter © 2012 Elsevier Ltd. All rights reserved.
doi:10.1016/j.mcm.2012.11.024

One aspect is widely accepted, where carriers must be treated as quantum mechanical rather than classical objects. The second change is the need to consider the atomic granularity of the constituent material since atomistic effects such as surface/interface roughnesses, unintentional doping, crystal asymmetries and distortions of the crystal lattice start to affect device performance [9,10]. For example, the *Stranski–Krastanov* growth technique, which is widely used to grow InGaAs QDs of a symmetric shape (e.g. domes or pyramids) on a host GaAs layer [11–13], generally does not guarantee a perfect symmetry in QD geometries due to the inter-diffusion at the QD/host-layer interface and atomic discretization on a crystal lattice.

Continuum band models such as the parabolic effective mass [14] and $k \cdot p$ approach [15,16] have been popularly used in nanoelectronics modeling. Typically, however, they not only ignore atomistic resolution on crystal lattices, but also fail to capture the non-parabolicity in experimentally known band structures. While the accuracy in band structures is achievable with the use of *ab initio* methods such as Density Functional Theory [17], the computing cost is too high to be utilized in modeling of realistically sized systems which typically involve simulation domains of a few million atoms.

Tight-binding parameters and NEMO 3-D. To meet the compromise between the computing cost and modeling accuracy, we use the nearest-neighbor empirical tight-binding (TB) band model to describe device electronic structures [18]. The most sophisticated TB model uses a set of 10 localized orbital bases (s, s^*, 3 $\times$ p, and 5 $\times$ d) on realistic atomic grids (20 with spin interactions), where the parameter set is fitted to reproduce experimentally verified bandgaps, masses, non-parabolic dispersions, and strain behaviors of bulk materials using a global minimization procedure based on a genetic algorithm [19] and analytical insights [20]. Computational practicality of the $sp^3d^5s^*$ TB approach has been proven with our well-established 3-D NanoElectronics MOdeling Tool (NEMO 3-D) work [10]. Developed with MPI/C to be used on high performance (HPC) computing clusters, NEMO 3-D can handle the strain and electronic structure calculations up to a simulation domain of 10^6 nm^3 that consists of 52 million atoms and involves a complex Hamiltonian matrix over one billion degrees of freedom (DOFs).

The validity of our TB approach has been established well through various simulation projects connected to experiments. Our $sp^3d^5s^*$ parameters have been extensively utilized to model the InGaAs/InAlAs resonant tunneling diode at high bias and high current [21], valley-splitting in miscut Si quantum wells on SiGe substrates [22], electron transport in InAs High Electron Mobility Transistors (HEMT) [23], gate-induced Stark effect [24] and transition of quantum confinements of a single phosphorus ion in the Si FinFET [25]. With a recent expansion in NEMO 3-D functionalities [26,27], we have also proven experimentally observed ohmic conduction in ultra-thin, highly phosphorus δ-doped nanowires in Si bulk [28], and confirmed the first physical realization of the single phosphorus atom transistor by reproducing experimentally measured Coulomb diamond patterns [29].

Objectives of this work. In spite of its extensive utilization in various modeling projects, the functionality of the original NEMO 3-D code is limited to electronic structure calculations, e.g. solving a 3-D Schrödinger equation to find single electron states in quantum dot, wire, well and bulk systems with a user-defined electric field if needed. We have therefore expanded the capability of the old NEMO 3-D to support: (I) a 3-D Poisson calculation for Schrödinger–Poisson self-consistent simulations [26,27], (II) the multi-subband Contact Block Reduction method for ballistic quantum transport simulations [30], and (III) the evaluation of the momentum matrix for simulations of inter-band light transitions in nanoscale devices [31].

The main objective of this work is to study TCAD simulations of optoelectronics. Of all the above-mentioned TCAD features newly developed, we provide a detailed discussion with a focus on the calculation of the momentum matrix, and demonstrate the usefulness of our in-house software, which has been developed as extensions of *NEMO 3-D peta* [32], as an optoelectronics TCAD with the following steps: (I) we first present a detailed description of the simulation methodology, (II) then validate the suggested methodology via simulations of small GaAs QDs with a focus on a proof of principle, and (III) move the simulation scope to realistically sized self-assembled InAs/GaAs dome-shaped QDs to seek the possibility of optimization of optical properties via the size-engineering of QDs. Then, as a secondary but a bit separated topic, we provide a brief introduction of our web-based environment for TCAD simulations that is developed to support online education and research in nanoelectronics in the Republic of Korea.

We note that a full methodological description of TB simulations for optoelectronics is presented in this work for the first time. This work thus serves as an useful document for other researchers who want to build their own TCAD software, where the analyses performed regarding the QD size-engineering are also useful as guidance in potential device designs. Through a technological introduction of the EDISION project, this work provides a good chance of learning about the ongoing science gateway project in the Republic of Korea.

2. Methodology

Understanding the theoretical and simulation details should be always the first and most essential step for modeling engineers to perform accurate calculations to support experimentalists for potential device designs. In this section, we thus provide a detailed description about the simulation methodology used in this work, focusing on the following three subsections: (I) computation of long-range strain and electronic structure calculations, (II) calculation of electrical polarization that is generated due to the crystal symmetry in finite heterostructures, and (III) calculation of optical matrix elements and its utilization to evaluate the strengths of light transitions.

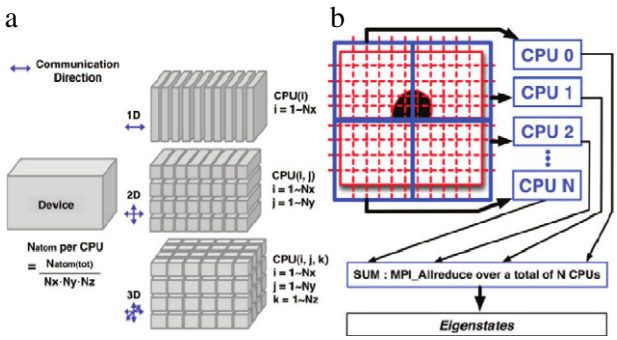

Fig. 1. (Color online) (a) Schematic of the 3-D spatial decomposition of the device geometry. (b) Illustration describing the scheme of the geometry parallelization that is utilized for simulations in this work.

2.1. Electronic structure and strain calculation

Electronic structure. Atomistic features of InAs/GaAs QDs are quantitatively explored with a TB band model. The single-particle energies and wavefunctions are calculated using an empirical set of 20-band $sp^3d^5s^*$ parameters with a consideration of the spin–orbit coupling. The underlying idea of this approach is the selection of a basis consisting of localized atomic orbitals (s, p, d, and s*) centered on each atom to reproduce experimentally known bulk mass and dispersion, and is conceptually more suitable to represent the finitely confined structures than the usage of plane-wave bases, which is used in the pseudo-potential method [33], and is more suitable for the description of infinite structures with periodic boundary conditions.

Calculation of single-particle energies and corresponding density of states (wavefunctions) involves a normal eigenvalue problem (Eq. (1)):

$$E\Psi = H\Psi, \tag{1}$$

where H is the complex Hermitian Hamiltonian matrix that represents the 3-D device geometries, Ψ is the wavefunction on a single-particle state, and E is the single-particle energy of the corresponding state. DOFs of the Hamiltonian matrix are equal to (the number of atoms in the device geometry) × (the number of orbital bases to represent a single atom), and thus typically become a few tens of millions if the structure has multi-million atoms. To handle these massive normal eigenvalue problems on peta-scale supercomputers [34], we have built an iterative solver based on the well-known LANCZOS algorithm [35] with an adoption of a parallelizing scheme that decomposes the device geometry spatially in a 3-D manner [36] as shown in Fig. 1.

Strain calculations. Semiconducting materials making up QDs may have different lattice constants; in a InAs/GaAs heterostructure, the lattice constants of InAs and GaAs are different with a 7% deviation (GaAs = 0.56532 nm, InAs = 0.60583 nm). Such a *lattice mismatch* causes a distortion of the original structures, leading to the appearance of strain tensors that cause displacements of atoms from their *ordered* positions in zinc-blende crystalline bulks. It's quite clear that the electronic properties of QD structures will be subjected to the atomic distortion stemming from the lattice mismatch, and the effect will become more serious as the device size becomes smaller, since the region subjected to atomic distortions will form a larger fraction of the entire device structure. The computation of strain should be therefore a critical step in simulations of nanoscale devices.

Strain field and distortion of each atomic placement are calculated with the well-known Valence Force Field (VFF) method and the Keating potential [37]. Here, the total mechanical energy of a system is interpreted as a sum of the elastic energy of bond distortions of each atom, e.g. like the elastic energy of springs connecting each atom. Then, the local strain energy at the nth atomic site, E_n, can be evaluated using Eqs. (2):

$$\begin{aligned} E_n &= A_n + B_n, \\ A_n &= \frac{3}{16}\sum_{m=1}^{k}\frac{\alpha_{n,m}}{d_{n,m}^2}(R_{n,m}^2 - d_{n,m}^2)^2, \\ B_n &= \frac{3}{8}\sum_{m=1}^{k}\sum_{l>m}^{k}\frac{\sqrt{\beta_{n,m}\beta_{n,l}}}{d_{n,m}d_{n,l}}(R_{n,m}R_{n.l} - d_{n,m}d_{n,l}), \end{aligned} \tag{2}$$

where k is the number of nearest neighbor atoms of the nth atom, and $d_{a,b}$ and $R_{a,b}$ represent the distance between the ath and bth atom at ordered crystalline (with no strain fields) and distorted systems, respectively. $\alpha_{a,b}$ and $\beta_{a,b}$ are the elastic constant of bonding between two atoms, which are also empirically determined to match experimentally known hydrostatic and biaxial strain behaviors of bulk materials [18,20]. Using the conjugate-gradient method [38], Eqs. (2) are then solved to find the displacement of each atom that achieves the minimum in the systematic energy. Once the set of *optimal* displacements is determined, the off-diagonal coupling blocks of the Hamiltonian matrix are modified with the displacement information, resulting in changes of electronic structures [10,39].

2.2. Piezoelectricity: electrical polarization

With no external bias applied, crystalline structures are supposed to be in charge neutrality. This charge neutrality, however, is not strictly conserved if structures are under stress, e.g. the entire structure maintains charge neutrality on average, but the charge neutrality may be broken on *local* atomic spots due to carrier movements. As a result, local dipoles (polarizations) may be formed, causing local (built-in) electric fields and voltage drops among local atomic spots. This is referred to as *piezoelectricity* [40] and sometimes becomes a critical step for the accurate simulation of nanoscale devices.

III–V compound materials such as GaAs, InAs, and GaN, are the very materials where the piezoelectricity affects electronic structures since they consist of atoms of different lattice constants and are thus subjected to spatial distortion and piezoelectric fields. Numerically, the strength of local polarizations can be described either by one parameter assuming a linearity between mechanical (strain) and electrical (piezoelectric) fields, or by a total of four parameters where we assume a quadratic relation between mechanical and electrical fields for better results [41,42]. In this work, we adopt the quadratic piezoelectricity and, given strain fields, the local polarization can be calculated with Eqs. (3)–(5):

$$\overrightarrow{P_1} = B_1 \begin{bmatrix} \epsilon_{yz} \\ \epsilon_{xz} \\ \epsilon_{xy} \end{bmatrix}, \tag{3}$$

$$\overrightarrow{P_2} = B_2 \begin{bmatrix} \epsilon_{xx}\epsilon_{yz} \\ \epsilon_{yy}\epsilon_{xz} \\ \epsilon_{zz}\epsilon_{xy} \end{bmatrix} + 2B_3 \begin{bmatrix} \epsilon_{xz}\epsilon_{xy} \\ \epsilon_{yz}\epsilon_{xy} \\ \epsilon_{yz}\epsilon_{xz} \end{bmatrix} + B_4 \begin{bmatrix} \epsilon_{yz}(\epsilon_{yy}+\epsilon_{zz}) \\ \epsilon_{xz}(\epsilon_{zz}+\epsilon_{xx}) \\ \epsilon_{xy}(\epsilon_{xx}+\epsilon_{yy}) \end{bmatrix}, \tag{4}$$

$$\overrightarrow{P} = 2(\overrightarrow{P_1} + \overrightarrow{P_2}), \tag{5}$$

where $(\epsilon_{xx}, \epsilon_{yy}, \epsilon_{zz}, \epsilon_{xy}, \epsilon_{xz}, \epsilon_{yz})$ are the six elements in a 3-D strain tensor matrix of each atom, (B_1, B_2, B_3, B_4) are the set of polarization constants for the quadratic piezoelectricity (known for GaAs and InAs, see Ref. [40]), and $\overrightarrow{P}$ is the polarization field on each atomic spot. Upon the obtained piezoelectric fields, the piezoelectric charge ρ and potential V can be evaluated using Gauss's law and Poisson's equation, respectively as shown in Eqs. (6):

$$\begin{aligned} \rho &= -\bigtriangledown \cdot \overrightarrow{P}, \\ \rho &= \epsilon_o \bigtriangledown \cdot [\epsilon_r \bigtriangledown V], \end{aligned} \tag{6}$$

where ϵ_o is the permittivity constant of air and ϵ_r is the relative permittivity of semiconducting materials. The calculated piezoelectric potential V is then added to diagonal sites of the Hamiltonian matrix creating a new Hamiltonian that represents a different electronic structure as shown in Eq. (7):

$$H' = H + V. \tag{7}$$

Before closing this subsection, we note that the 3-D Poisson equation is also solved by our in-house parallel code, where we used the AZTEC package [43] to solve a linear system iteratively, and the finite difference method [44] for the spatial discretization of simulation domains.

2.3. Momentum matrix and optical transition

As already mentioned in the previous section, the most important object of this work is to assess the potential utility of the self-assembled InAs/GaAs QDs as optoelectronic devices at infrared wavelengths, for which we need to evaluate band (optical) gaps, as well as the strength of corresponding inter-band light transitions. The optical gaps, however, have been already discussed many times in previous literature and well understood so far [10,45]. The strength of this work should be thus on the discussion of light transitions, which motivates a well-organized and detailed description of the related methodology. For this purpose, we first explain the methods that are originally known for bulk materials, then describe the changes needed by the original methodology for simulations of 3-D confined structures.

In bulk semiconductors. Let's assume two states, e.g. one is the state A that is fully occupied by an electron, and the other is the state B that is completely empty. The steady-state transition probability of a single electron from state A to B with a photon energy of $\hbar\omega$, $T_{A\to B}$, can then be evaluated by Eq. (8) following Fermi's golden rule [46]:

$$T_{A\to B} = \frac{2\pi}{\hbar} |\langle \psi_B \mid H \mid \psi_A \rangle|^2 \delta(\hbar\omega - (E_B - E_A)), \tag{8}$$

where (E_A, ψ_A) and (E_B, ψ_B) are the energy and wavefunction at state A and B, respectively, and H is the device Hamiltonian. If we assume E_B is larger than E_A, and the light energy is always large enough to make the transition happen, i.e. $\hbar\omega \geq (E_B - E_A)$, the expression in Eq. (8) can be further elaborated for bulk systems as shown in Eqs. (9). We note that states are now denoted

by corresponding wave vectors $(\overrightarrow{k_A}, \overrightarrow{k_B})$ within the 1st Brillouin Zone (BZ) of a single unit-cell:

$$\begin{aligned} T_{A\to B} &= \frac{2\pi}{\hbar}|\langle\psi_B \mid H \mid \psi_A\rangle|^2 \\ &= \frac{\pi q^2}{2\hbar m_o^2}\left|\int_{uc} d^3r\,\psi_{\overrightarrow{k_B}}(r)\frac{\hbar}{i}\bigtriangledown\cdot\overrightarrow{n}\,\psi_{\overrightarrow{k_A}}(r)\right|^2 \\ &= \frac{\pi q^2}{2\hbar m_o^2}|\overrightarrow{P}(\overrightarrow{k_A}, \overrightarrow{k_B})\cdot\overrightarrow{n}|^2, \end{aligned} \tag{9}$$

where $(\overrightarrow{k_A}, \overrightarrow{k_B})$ are the wave vectors at state A and B within the 1st BZ of a single unit-cell, $(\psi_{\overrightarrow{k_A}}, \psi_{\overrightarrow{k_B}})$ are corresponding wavefunctions, uc denotes the region of a single unit-cell, m_o is the free electron mass, $\overrightarrow{n}$ is the direction of the polarization induced by the incident light, and $\overrightarrow{P}(\overrightarrow{k_A}, \overrightarrow{k_B})$ is the element at state (A, B) of the momentum matrix. We note, given state energies and wavefunctions, the momentum matrix fully determines the strength of inter-state light transitions.

In 3-D confined structures. In bulks, electron and hole movement are normally interpreted as a plane-wave traveling in all 3-D spatial directions. This is, however, not true any more in QDs, since carrier movements are not free and should be interpreted as *standing waves* with a set of selectively available wave vectors. For a rectangular-shaped QD box, the collection of available wave vectors becomes:

$$\begin{aligned} \overrightarrow{k} &= (k_x, k_y, k_z) \\ &= \left(\frac{n_x\pi}{L_x}, \frac{n_y\pi}{L_y}, \frac{n_z\pi}{L_z}\right), \end{aligned} \tag{10}$$

where (L_x, L_y, L_z) are dimensions of the QD box along 3-D spatial directions, and (n_x, n_y, n_z) are a set of principal quantum numbers. Since we only consider the 1st BZ of the QD box, elements of the wave vector, (k_x, k_y, k_z) should satisfy the following condition:

$$0 \le \{k_x, k_y, k_z\} < \left\{\frac{\pi}{L_x}, \frac{\pi}{L_y}, \frac{\pi}{L_y}\right\}, \tag{11}$$

where the only available combination of (k_x, k_y, k_z) becomes $(0, 0, 0)$ within the 1st BZ of the QD box, indicating the net momentum of carrier waves is effectively zero in 3-D confined structures. The momentum matrix $\overrightarrow{P}$ in Eqs. (9) needs to be evaluated only at the Γ point with a focus on the state energy (E_A, E_B):

$$\begin{aligned} \overrightarrow{P}(\overrightarrow{k_A}, \overrightarrow{k_B}) &= \overrightarrow{P}(E_A, E_B)|_{\overrightarrow{k}=\overrightarrow{0}} \\ &= (P_x, P_y, P_z), \end{aligned} \tag{12}$$

$$P_x = \int_{uc} d^3r\,\psi_{E_B}(r)\frac{\hbar}{i}\bigtriangledown\cdot\overrightarrow{e_x}\,\psi_{E_A}(r), \tag{13}$$

$$P_y = \int_{uc} d^3r\,\psi_{E_B}(r)\frac{\hbar}{i}\bigtriangledown\cdot\overrightarrow{e_y}\,\psi_{E_A}(r),$$

$$P_z = \int_{uc} d^3r\,\psi_{E_B}(r)\frac{\hbar}{i}\bigtriangledown\cdot\overrightarrow{e_z}\,\psi_{E_A}(r),$$

where $\{\overrightarrow{e_x}, \overrightarrow{e_y}, \overrightarrow{e_z}\}$ are unit element vectors along the spatial x, y, and z directions. Numerically, vector elements of the momentum matrix, (P_x, P_y, P_z) in Eq. (13), can be evaluated as:

$$\begin{aligned} P_x &= \frac{im_o}{\hbar}\langle\psi_{E_B}|[H, x]|\psi_{E_A}\rangle \\ &= \frac{im_o}{\hbar}\langle\psi_{E_B}|(Hx - xH)|\psi_{E_A}\rangle \\ &= \frac{im_o}{\hbar}\left[\langle\psi_{E_B}|Hx|\psi_{E_A}\rangle - \langle\psi_{E_B}|xH|\psi_{E_A}\rangle\right], \end{aligned} \tag{14}$$

where the vector elements are calculated via the commutator relation [47,48], and x is the position on the x-axis of atoms in the device structure. We note that only P_x is shown in Eqs. (14) to save space. P_y and P_z can be calculated exactly in the same manner, except that we need to use atomic positions on y and z positions, respectively. For an arbitrary direction $\overrightarrow{n} = (n_x, n_y, n_z)$ of light-induced polarization, now the transition probability $T_{A\to B}$ can be evaluated using Eqs. (15):

$$\begin{aligned} T_{A\to B} &\sim |\overrightarrow{P}(\overrightarrow{E_A}, \overrightarrow{E_B})\cdot\overrightarrow{n}|^2 \\ &= |(P_x, P_y, P_z)\cdot(n_x, n_y, n_z)|^2 \\ &= |P_x n_x + P_y n_y + P_z n_z|^2. \end{aligned} \tag{15}$$

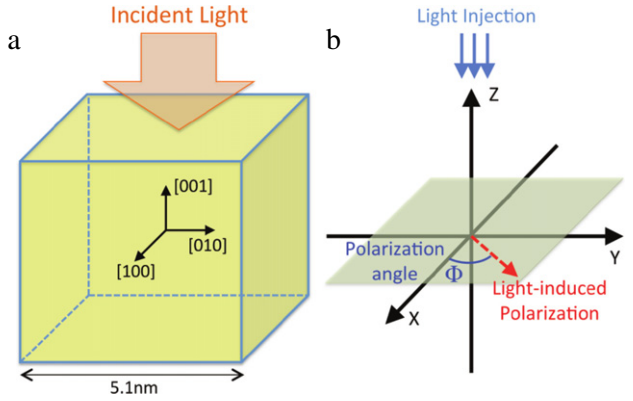

Fig. 2. (Color online) (a) Schematic of the 5.1 nm cubic GaAs QD to be simulated for the validation of simulation methodologies. Light is assumed to be injected from the top. (b) Illustration representing the direction of light-induced polarizations.

3. Results and discussions

3.1. Validation: simulation methodology

Simulation target. To validate the methodological details presented in the previous section via Eqs. (1)–(15), we simulate the GaAs rectangular box QD as shown in Fig. 2(a). The QD structure is assumed to be grown along the [001] direction, and hard-wall boundary conditions are applied to all the surface atoms by passivating their dangling bonds [49]. The simulation domain as a result becomes a 5.1 nm × 5.1 nm × 5.1 nm (9 unit-cells along each axis) box that contains a total of 5832 atoms and involves a complex Hermitian Hamiltonian matrix of 116,640 DOFs due to the usage of 20 bands per each atom. The light is assumed to be injected from the top ([001] direction).

Light-induced polarization. From the electromagnetic theory [50], it is well understood that a traveling light wave creates electric fields around itself such that electrical polarizations happen along any directions perpendicular to the direction of the light propagation. In the simulation target, the light-induced polarizations should thus happen on the (001) plane as we assumed the light injection happens along the [001] direction, e.g. the light-induced polarization can happen at any Φ's between 0° and 360° (Fig. 2(b)).

Simulation results. With a set of 20 localized orbital bases proposed by Jancu et al. [51], the $sp^3d^5s^*$ TB model reproduces the experimentally verified GaAs bulk band structure quite well, locating the bulk conduction band minimum (CBM) and valence band maximum (VBM) at ∼1.424 eV and ∼0.03 eV, respectively, where the zero energy represents the Si bulk VBM. The electron and hole ground states in the target QD structure, however, are shifted up and down with respect to the bulk CBM and VBM, respectively, due to the 3-D confinement of the geometry. The QD electron (E1) and hole ground state (H1) are thus placed at around 1.77 eV and −0.12 eV, respectively, creating an optical gap of ∼1.90 eV.

Top views of the 3-D wavefunction on E1 and H1 states are illustrated in Fig. 3(a). Here, the conduction band ground state has a wavefunction that is almost circular and symmetric with respect to the center on the (001) plane. The wavefunction E1 is, however, not perfectly symmetric because of the asymmetry in the QD structure, which is called the *crystal asymmetry* and is due to a 'zig–zag' distribution of atoms in the zinc-blende crystal and the difference in atomic species, as illustrated in Fig. 3(b). The wavefunction on the valence band ground state is also asymmetric, where the wavefunction is elongated along the [110] direction (tilted by ∼45° with respect to the [100] direction).

Given the direction of a light-induced polarization and an assumption of no traps in the device structure, the strength of the ground state inter-band optical transition is proportional to the ground state band-to-band recombination rate along the polarization direction, where the recombination rate is again directly proportional to a multiplication of the electron and hole density on the conduction and valence band ground state, respectively [52]. Since the uniform volume density of electrons and holes cannot be assumed any more in nanoscale devices, the band-to-band recombination rate R(E1, H1) should be interpreted in terms of carrier wavefunctions (Eq. (16)):

$$R(\mathrm{E1, H1}) \propto \int_{\vec{n}} dr |\Psi_{\mathrm{E1}}(r)|^2 |\Psi_{\mathrm{H1}}(r)|^2, \tag{16}$$

where the right term represents a *line integral* along a direction of the light-induced polarization. Here the absolute square of a wavefunction becomes the carrier distribution such that the $|\Psi_{\mathrm{H1}}|^2$ also represents a local hole distribution although Ψ_{H1} itself means an electron wavefunction, i.e. electron and hole distribution on a state should be the same, since a hole is an empty electron.

Fig. 3(c) shows the polarization-dependent strength of ground state inter-band optical transitions, where the maximum value is normalized to one. Sweeping Φ (Fig. 2(b)) from 0° to 360° to model arbitrary light-induced polarizations on the (001) plane, we can easily expect the transition strength should be maximized at Φ of ∼45 (and 45 + 180) degrees and minimized

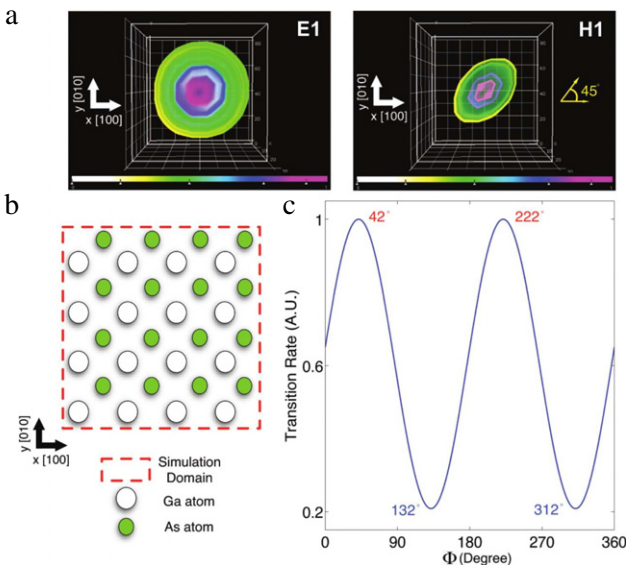

Fig. 3. (Color online) (a) Wavefunctions at electron ground state (E1: 1.77 eV) and hole ground state (H1: −0.12 eV). Both the wavefunctions E1 and H1 are not perfectly symmetric due to the crystal asymmetry in the QD structure. The hole wavefunction (H1) shows much larger asymmetry, being elongated along the [110] direction. (b) Conceptual illustration of the crystal asymmetry on the (001) GaAs plane. Note that the view from the left and right sides are not the same. (c) The strength of inter-band light transition normalized to the maximum value. The strength reaches its maximum and minimum at Φ of 42° and 132°, respectively.

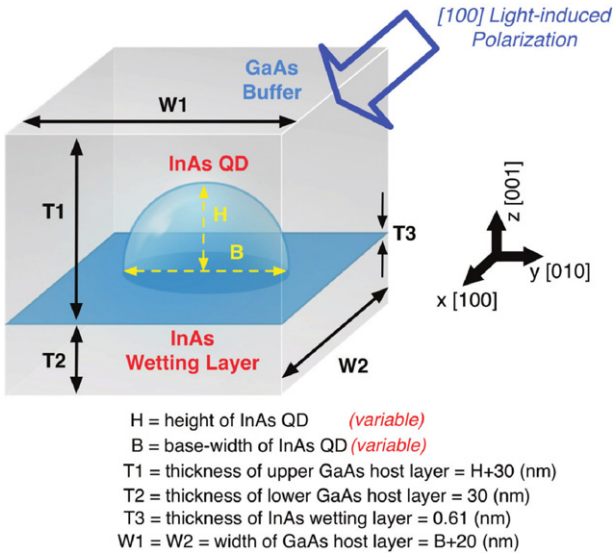

Fig. 4. (Color online) Schematic view of a single dome-shaped InAs QD in the GaAs host layer. Simulations are performed for various heights (H) and base-widths (B) of the InAs QDs to investigate the possibility to maximize the strength of the optical transition via size-engineering. The dome-shaped InAs QD is grown on a single unit-cell thick InAs wetting layer and encapsulated by a 30 and 10 nm thick GaAs buffer along the [100]/[010] and [001] direction, respectively.

at ∼135 (and 135 + 180) degrees, since the line integral in Eq. (16) reaches its maximum and minimum at corresponding angles. The sinusoidal pattern of the transition strength in Fig. 3(c) clearly supports the discussion we have made so far, validating the simulation methodology presented in the previous section.

3.2. TCAD simulation of optical properties: dome-shaped InAs quantum dot in GaAs layer

Simulation target. Upon a validation of the simulation methodology presented in the previous subsection, we now move the scope of simulations to realistically sized systems. Fig. 4 depicts the schematic of the InAs/GaAs QD system simulated

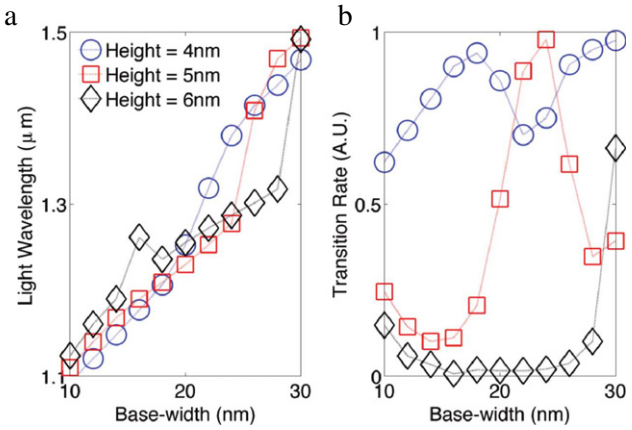

Fig. 5. (Color online) (a) Optical properties of dome-shaped InAs QDs in a host GaAs buffer: optical gaps represented as the light wavelength. (b) Strengths of the ground state inter-band light transition.

to investigate optical properties, where a dome-shaped InAs QD of a height H and a base width B is on a single unit-cell thick InAs wetting layer and embedded in a GaAs box of hard-wall boundaries. In reality, the dome-shaped single InAs QD is grown on a thin InAs wetting layer and a GaAs host material by Low-Pressure Metal-Organic Chemical Vapor Deposition (LPMOCVD) [2], and the QD is completely encapsulated by bulk-like GaAs layers. It is, however, impossible to consider bulk-like GaAs layers in the simulation domain due to an expensive computing cost such that we use a 10 and 30 nm thickness of GaAs layers along the [100]/[010] and [001] directions, respectively, which turn out to be thick enough to represent bulk-like layers since a further increase of thickness does not shift the energetic positions of the electron and hole ground state for all the InAs QD samples simulated in this work.

As mentioned in the first section, one objective of this work is to seek for the possibility of size-engineering of QD optical properties. For this purpose, optical gaps and ground state inter-band transitions under a [100] light-induced polarization are simulated for a total of 33 different QD sizes, where we consider three different H's (4, 5, 6 nm) and eleven B's (from 10 to 30 nm with a step of 2 nm) for each H. All the simulations have been performed on a 64-bit, 8-core SUN Blade 6275 system of 24 GB SDRAM and infiniband ($4 \times$ QDR) interconnect local to each node (TACHYON-II HPC cluster operated by the supercomputing center of the Korea Institute of Science and Technology Information). Device electronic structures simulated in this work consist of 2.5∼7.2 million atoms, and require 128 cores for 4∼19 h for calculations depending on the dimensions of InAs QDs.

Size-engineering of optical properties. Fig. 5 demonstrates optical properties of various dome-shaped QDs, where we have plotted inter-band optical gaps and ground state inter-band light transition rates as functions of QD size. In terms of optical gaps that are represented in units of light wavelength rather than energy for convenience in the discussion, InAs QDs exhibit light wavelengths that are much smaller than the wavelength observed from a InAs bulk band gap (∼3.2 μm, ∼0.4 eV), due to the 3-D spatial confinement created by GaAs host layers. This structural confinement of InAs QDs becomes weaker with increasing QD sizes, causing a reduction in the optical gap and an increase in the light wavelength. As far as the optical gap is concerned, we may conclude that most of the QD samples simulated in this work are quite useful as optoelectronics at the infrared wavelength ($\gtrsim$1.2 μm).

Although the pattern of simulated optical wavelengths shows a clear dependency on QD sizes and looks quite reasonable, the result of inter-band light transition rates claims that the true utility of QD systems as optoelectronics cannot be solely determined only by the optical gap since light transitions are extremely weak in some QD devices as indicated in Fig. 5(b), where transition strengths are shown being normalized to the maximum value of all 33 simulation cases. Differently from the optical gap, the transition rate does not show a consistent dependency on the QD size such that finding a control factor to increase the light transition rate should be a critical step needed for the guidance of potential device designs.

To continue discussions, we narrow the range of analyses by reducing DOFs of the simulation data set. Fig. 6 shows the transition rate and the [100] line integral of the spatial overlap of wavefunctions on the electron (E1) and hole ground states (H1) as a function of the QD base-width, where the QD height is fixed to 5 nm. Here, we observe that the transition rate shows a clear local maximum with an increasing base-width (or a decreasing aspect-ratio), and that the pattern is quite close to the variation of the spatial overlap of ground state wavefunctions that represents the local electron–hole recombination rate as discussed in Eq. (16).

Fig. 6(b) shows spatial distributions of the E1 and H1 wavefunction for the three base-widths of 14, 24 and 30 nm. While the electron ground state wavefunctions have almost symmetric (sphere-like) shapes regardless of the QD aspect-ratio due to the s-orbital-like symmetry, the shapes of hole ground state wavefunctions are quite sensitive to the geometry due to the strain and piezoelectric field induced symmetry breaking [45,53]. At the base-width of 14 nm, the hole wavefunction is mostly oriented along the [001] direction due to the large aspect-ratio of InAs QD, causing a small spatial overlap of the two

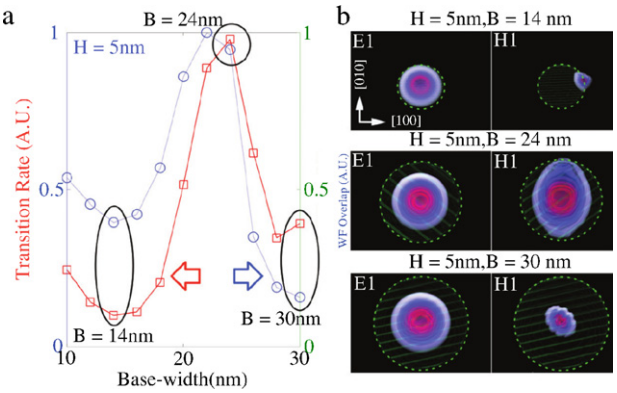

Fig. 6. (Color online) (a) The light transition rate and spatial overlap of the wavefunction on E1 and H1 states along the [100] direction are plotted as a function of the QD base-width at a 5 nm height. (b) Top views of the wavefunction on E1 and H1 states for base-widths of 14, 24 and 30 nm, where green dotted lines describe the edges of QD bases. While electron wavefunctions (E1) show symmetric shapes for all the cases, shapes of hole wavefunctions (H1) are sensitive to the QD aspect-ratio, creating the local maximum of the transition rate.

wavefunctions on the (001) plane. When the base-width increases to 24 nm, the hole wavefunction spreads over the (001) plane, increasing the spatial overlap along the [100] direction. Finally, for a larger base-width at 28 nm, the QD becomes almost flat with very low aspect-ratio. In this case, the strain induced symmetry breaking determines the spatial alignment of the ground state hole wavefunctions and the spatial overlap again decreases due to alignment of the hole wavefunction along the [110] direction.

We note that the discussion on the spatial distribution of wavefunctions not only shows that the wavefunction of the hole ground state becomes a critical factor that controls the inter-band transition strength, but also reveals an important point in QD designs that the optical transition strength could be engineered by changing the QD aspect-ratio.

3.3. Web-based environment for science simulation

Needs for science gateway. TCAD simulations these days commonly require a huge computing cost [10,30,36]. Computational scientists thus increasingly use web portals and various stand-alone applications (e.g. Terminal) as gateways to access computational resources and TCAD packages that are integrated with HPC clusters, motivating the strong needs for a *Science Gateway* [54,55], of which the concept is defined as a community-specific set of tools, applications, and data collections that are integrated via a portal or a suite of applications, providing access to HPC-integrated resources. The nanoHUB.org project led under the financial support of US National Science Foundation (NSF) [56–59], is one good example showing the strong needs for such science gateways.

Based on the well-known strong national competitiveness in the semiconducting industry and IT infrastructure in the Republic of Korea, we have recently launched the 'EDucation-research Integration through Simulation On the Net' (EDISON) project under the financial support of the Ministry of Education, Science and Technology of the Republic of Korea, where the main goal of the project is to construct a web-based cyber infrastructure to support education and research via nanoelectronics simulations. In this subsection, we briefly introduce the technological aspect of our ongoing project.

System architecture. Fig. 7 describes a high level system architecture of the web-based simulation environment that we have developed. To perform simulations via a web-portal (Simulation Portal), users start on creating their own workflows for simulations (via a Simulation User Interface (UI)), where the workflow consists of three steps: pre-processing, simulation-running, and post-processing [60]. Here the simulation workflow can be either directly edited by users, or be retrieved from the repository (Science AppStore) if the same workflow has been already utilized. Once the simulation is launched, users can not only monitor the status of their own work but also visualize the simulation results. Various management UIs equipped in the simulation portal allow the system administrator to manage the user account, virtual resources, and the system itself as well.

The simulation portal is run on top of the four middleware components composed of 'Science AppStore', 'Simulation Management', 'Credential Management', and 'Virtual Resource Management', where each component can be explained in detail as follows: (I) Science AppStore is a repository that contains various executables of TCAD simulators, simulation-specific metadata such as input and output file formats, and administrative functionalities. (II) Simulation Management stores the provenance and run-time data during job executions. Functionalities of submitting and monitoring jobs on backward HPC clusters are presented here. (III) Users are authenticated via our Credential Management Services, for which we use the open software MyProxy [61] that is based on the Grid Security Infrastructure (GSI) [62]. (4) Virtual Resource Management provides functionalities of the on-demand provisioning, job authentication and management for virtual resources, and administrative tools. All the middleware components run on physical computing clusters (Computing Resources).

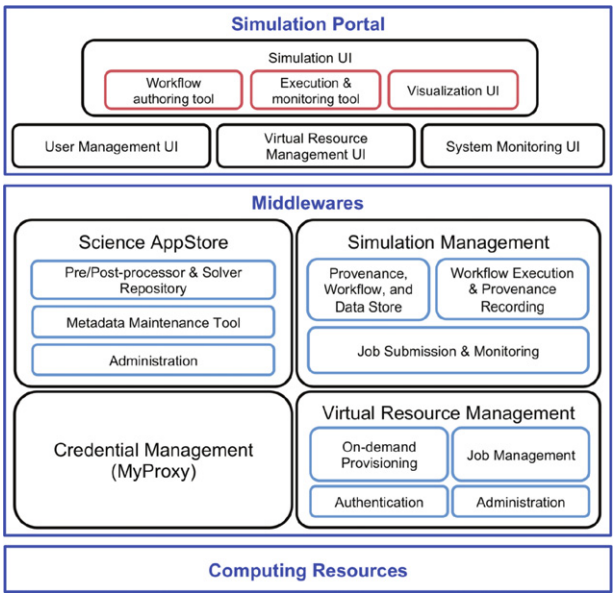

Fig. 7. (Color online) Illustration of the system architecture of the web-based environment for TCAD simulations (EDISON platform). The platform consists of three layers: a simulation portal that supports user-friendly graphical interfaces for simulation setups, middleware components, and physical computing resources.

4. Conclusion

We carefully examine optical properties of InAs/GaAs quantum dots (QDs) in a modeling perspective. Electronic structures of QDs are represented with the atomistic 20-band $sp^3d^5s^*$ tight-binding (TB) approach, and state-quantizations in 3-D confined structures are calculated with consideration of the piezoelectric potential and long-range atomic distortions that are stemming from a mismatch of the lattice constant of bulk GaAs and InAs. All the simulations are performed with our in-house TCAD solver that has been developed as extensions of *NEMO* 3-*D peta* to be utilized on supercomputing clusters.

To our knowledge, this work provides a full summary on the methodology of TB simulations of light transitions for the first time. To validate the suggested methodology with a focus on a proof of principle, we simulate a small GaAs box QD and show that the strength of a two-state light transition is perfectly proportional to the spatial overlap of the wavefunction on the initial and final state. Then, we move the simulation scope to a realistically sized dome-shaped single InAs QD in a host GaAs buffer, where we not only show that the strength of ground state inter-band light transitions can be optimized by an engineering of QD aspect-ratios, but also observe that the hole ground state wavefunction plays a key role in the determination of transition strengths.

We finish the paper with a brief introduction of the government-supported EDucation-research Integration through Simulation On the Net (EDISON) project, where we present a technological description of the high-level system architecture of our web-based environment that is developed to support education and research in nanoelectronics via online TCAD simulations.

Acknowledgments

TACHYON-II supercomputing clusters at the Korea Institute of Science and Technology Information (KISTI), and US NSF-supported nanoHUB.org computing resources have been extensively used in this work. A part of this work has been carried out under support by the EDucation-research Integration through Simulation On the Net (EDISON) project funded by the Ministry of Education, Science and Technology, Republic of Korea (contract number N-11-NM-IR11). HR and GK thankfully acknowledges fruitful comments from Prof. Timothy B. Boykin (University of Alabama in Huntsville). HR would like to dedicate this paper to J.H. Sohn in appreciation of her consistent support and encouragement for research.

References

[1] D.L. Huffaker, G. Park, Z. Zou, O.B. Shchekin, D.G. Deppe, 1.3 μm room-temperature GaAs-based quantum-dot laser, Appl. Phys. Lett. 73 (1998) 2564.
[2] F. Koyama, D. Schlenker, T. Miyamoto, Z. Chen, K. Iga, 1.2 μm GaInAs/GaAs lasers: are they useful for high-capacity single-mode fiber datacom? in: Proc. of SPIE, vol. 3899, 1999, p. 290.
[3] J. Tatebayashi, M. Nishioka, Y. Arakawa, Over 1.5 μm light emission from InAs quantum dots embedded in InGaAs strain-reducing layer grown by metalorganic chemical vapor deposition, Appl. Phys. Lett. 78 (2001) 3469.
[4] D. Pan, E. Towe, S. Kennerly, Normal-incidence intersubband (In, Ga)As/GaAs quantum dot infrared photodetectors, Appl. Phys. Lett. 73 (1998) 1937.

[5] P. Jayavel, H. Tanaka, T. Kita, O. Wada, H. Ebe, M. Sugawara, J. Tatebayashi, Y. Arakawa, Y. Nakata, T. Akiyama, Control of optical polarization anisotropy in edge emitting luminescence of InAs/GaAs self-assembled quantum dots, Appl. Phys. Lett. 84 (2004) 1820.
[6] L. Fortunato, M.T. Todaro, V. Tasco, M.D. Giorgi, M.D. Vittorio, R. Cingolani, A. Passaseo, Control of unpolarized emission in closely stacked InAs quantum dot structure, Superlattices Microstruct. 47 (2010) 72–77.
[7] R.P. Mirin, J.P. Ibbetson, K. Nishi, A.C. Gossard, J.E. Bowers, 1.3 μm photoluminescence from InGaAs quantum dots on GaAs, Appl. Phys. Lett. 67 (1996) 3795.
[8] G.E. Moore, Gramming more components onto integrated circuit, Electronics 38 (8) (1965) 114–117.
[9] T. Shinada, S. Okamoto, T. Kobayashi, J.R. Barker, I. Ohdomari, Enhancing semiconductor device performance using ordered dopant arrays, Nature 437 (2005) 1128–1131.
[10] G. Klimeck, S.S. Ahmed, H. Bae, N. Kharche, R. Rahman, S. Clark, B. Haley, S. Lee, M. Naumov, H. Ryu, F. Saied, M. Prada, M. Korkusinski, T.B. Boykin, Atomistic simulation of realistically sized nanodevices using NEMO 3-D: PART I—models and benchmarks, IEEE Trans. Electron Devices 54 (2007) 2079–2089.
[11] M. Petroff, Single Quantum Dots: Fundamentals, Applications, and New Concepts, Springer-Berlin, 2003.
[12] M.A. Reed, J.N. Randall, R.J. Aggarwal, R.J. Matyi, T.M. Moore, A.E. Wetsel, Observation of discrete electronic states in a zero-dimensional semiconductor nanostructure, Phys. Rev. Lett. 60 (1988) 535.
[13] G. Bester, A. Zunger, Cylindrically shaped zinc-blende semi-conductor quantum dots do not have cylindrical symmetry: atomistic symmetry, atomic relaxation, and piezoelectric effects, Phys. Rev. B 71 (2005) 045318.
[14] C. Pryor, J. Kim, L.W. Wang, A.J. Williamson, A. Zunger, Comparison of two methods for describing the strain profiles in quantum dots, J. Appl. Phys. 83 (1998) 2548.
[15] M. Grundmann, O. Stier, D. Bimberg, InAs/GaAs pyramidal quantum dots: strain distribution, optical phonons, and electronic structure, Phys. Rev. B 52 (1995) 011969.
[16] O. Stier, M. Grundmann, D. Bimberg, Electronic and optical properties of strained quantum dots modeled by 8-band $k \cdot p$ theory, Phys. Rev. B 59 (1999) 5688.
[17] D.J. Carter, O. Warschkow, N.A. Marks, D.R. McKenzie, Electronic structure models of phosphorus δ-doped silicon, Phys. Rev. B 79 (2009) 033204.
[18] G. Klimeck, F. Oyafuso, T. Boykin, R. Bowen, P. vonAllmen, Development of a nanoelectronic 3-D (NEMO 3-D) simulator for multimillion atom simulations and its application to alloyed quantum dots, Comput. Model. Eng. Sci. 3 (2002) 601–642.
[19] G. Klimeck, R.C. Bowen, T.B. Boykin, C.S. Lazaro, T.A. Cwik, A. Stoica, Si tight-binding parameters from genetic algorithm fitting, Superlattices Microstruct. 27 (2000) 77–88.
[20] T.B. Boykin, G. Klimeck, R.C. Bowen, F. Oyafuso, Diagonal parameter shifts due to nearest-neighbor displacements in empirical tight-binding theory, Phys. Rev. B 66 (2002) 125207.
[21] R.C. Bowen, G. Klimeck, R.K. Lake, W.R. Frensley, T. Moise, Quantitative simulation of a resonant tunneling diode, J. Appl. Phys. 81 (1997) 3207.
[22] N. Kharche, M. Prada, T.B. Boykin, G. Klimeck, Valley-splitting in strained silicon quantum wells modeled with 2° miscuts, step disorder, and alloy disorder, Appl. Phys. Lett. 90 (2007) 9.
[23] N. Kharche, G. Klimeck, D.H. Kim, J.A. del Alamo, M. Luisier, Performance analysis of ultra-scaled InAs HEMTs, in: Proceedings of IEEE IEDM, 2009.
[24] R. Rahman, C.J. Wellard, F.R. Bradbury, M. Prada, J.H. Cole, G. Klimeck, L.C.L. Hollenberg, High precision quantum control of single donor spins in silicon, Phys. Rev. Lett. 99 (2007) 036403.
[25] G.P. Lansbergen, R. Rahman, C.J. Wellard, I. Woo, J. Caro, N. Collaert, S. Biesemans, G. Klimeck, L.C.L. Hollenberg, S. Rogge, Gate-induced quantum-confinement transition of a single dopant atom in a silicon FinFET, Nature Phys. 4 (2008) 656–661.
[26] H. Ryu, S. Lee, G. Klimeck, A study of temperature-dependent properties of n-type δ-doped Si bandstructures in equilibrium, in: Proc. of IEEE International Workshop on Computational Electronics, IWCE, 2009.
[27] H. Ryu, S. Lee, B. Weber, S. Mahapatra, M.Y. Simmons, L.C.L. Hollenberg, G. Klimeck, Quantum transport in ultra-scaled phosphorus-doped silicon nanowires, in: Proc. of IEEE Silicon Nanoelectronics Workshop, 2010.
[28] B. Weber, S. Mahapatra, H. Ryu, S. Lee, A. Fuhrer, T.C.G. Reusch, D.L. Thompson, W.C.T. Lee, G. Klimeck, L.C.L. Hollenberg, M.Y. Simmons, Ohm's law survives to the atomic scale, Science 335 (2012) 64–67.
[29] M. Fuechsle, J.A. Miwa, S. Mahapatra, H. Ryu, S. Lee, O. Warschkow, L.C.L. Hollenberg, G. Klimeck, M.Y. Simmons, A single-atom transistor, Nature Nanotech. (2012) http://dx.doi.org/10.1038/nnano.2012.21. Advanced Online Publication.
[30] H. Ryu, H.H. Park, M. Shin, D. Vasileska, G. Klimeck, Feasibility, accuracy and performance of contact block reduction method for multi-band simulations of ballistic quantum transport, J. Appl. Phys. 111 (2012) 063705.
[31] H. Ryu, M. Usman, S. Lee, Y.H. Tan, G. Klimeck, Quantum confined stark shift and ground state optical transition rate in [100] laterally biased InAs/GaAs quantum dots, in: Proc. of IEEE International Workshop on Computational Electronics, IWCE, 2009.
[32] S. Lee, H. Ryu, H. Campbell, L.C.L. Hollenberg, M.Y. Simmons, G. Klimeck, Electronic structure of realistically extended atomistically resolved disordered Si:P δ-doped layers, Phys. Rev. B. 84 (2011) 205309.
[33] A. Canning, L.W. Wang, A. Williamson, A. Zunger, Parallel empirical pseudopotential electronic structure calculations for million atom systems, J. Comput. Phys. 160 (2000) 29–41.
[34] See http://www.top500.org for the list of worldwide top 500 supercomputing clusters.
[35] C. Lanczos, An iteration method for the solution of the eigenvalue problem of linear differential and integral operators, J. Res. Natl. Bur. Stand. 45 (1950) 255–282.
[36] S. Lee, H. Ryu, Z. Jiang, G. Klimeck, Million atom electronic structure and device calculations on peta-scale computers, in: Proc. of IEEE International Workshop on Computational Electronics, IWCE, 2009.
[37] P.N. Keating, Effect of invariance requirements on the elastic strain energy of crystals with application to the diamond structure, Phys. Rev. 145 (1966) 637–645.
[38] J.L. Nazareth, Computational Statistics, in: Wiley Interdisciplinary Reviews, vol. 1, 2009, pp. 348–353.
[39] T.B. Boykin, G. Klimeck, F. Oyafuso, Valence band effective-mass expressions in the $sp^3d^5s^*$ empirical tight-binding model applied to a Si and Ge parameterization, Phys. Rev. B 69 (2004) 115201.
[40] W.F. Cady, Piezoelectricity, McGraw-Hill, New York, 1946.
[41] G. Bester, A. Zunger, X. Wu, D. Vanderbilt, Effects of linear and nonlinear piezoelectricity on the electronic properties of InAs/GaAs quantum dots, Phys. Rev. B 74 (2006) 081305.
[42] A. Schliwa, M. Winkelnkemper, D. Bimberg, Impact of size, shape, and composition on piezoelectric effects and electronic properties of In(Ga)As/GaAs quantum dots, Phys. Rev. B 76 (2007) 205324.
[43] See http://www.cs.sandia.gov/CRF/aztec1.html for detailed information of the AZTEC package.
[44] R.J. Leveque, Finite Difference Methods for Ordinary and Partial Differential Equations: Steady-State and Time-Dependent Problems, Siam, 2007.
[45] M. Usman, H. Ryu, I. Woo, G. Klimeck, Moving toward Nano-TCAD through multimillion-atom quantum-dot simulations matching experimental data, IEEE Trans. Nanotechnology 8 (2009) 330–344.
[46] A. Szabo, N.S. Ostlund, Modern Quantum Chemistry: Introduction to Advanced Electronic Structure Theory, McGraw-Hill, New York, 1989.
[47] T.B. Boykin, R.C. Bowen, G. Klimeck, Electromagnetic coupling and gauge invariance in the empirical tight-binding method, Phys. Rev. B 63 (2001) 245314.
[48] T.B. Boykin, P. Vogl, Dielectric response of molecules in empirical tight-binding theory, Phys. Rev. B 65 (2001) 035202.
[49] S. Lee, F. Oyafuso, P. von Allmen, G. Klimeck, Boundary conditions for the electronic structure of finite-extent embedded semiconductor nanostructures, Phys. Rev. B 69 (2004) 045316.
[50] D.K. Cheng, Field and Wave Electromagnetics, second ed., Addition-Wesley, 1989.

[51] J.M. Jancu, R. Scholz, F. Beltram, F. Bassani, Empirical spds* tight-binding calculation for cubic semiconductors: general method and material parameters, Phys. Rev. B 57 (1998) 6493.
[52] R.F. Pierret, Semiconductor Device Fundamentals, Addison-Wesley, 1996.
[53] G.A. Narvaez, G. Bester, A. Zunger, Dependence of the electronic structure of self-assembled (In, Ga)As/GaAs quantum dots on height and composition, J. Appl. Phys. 98 (2005) 043708.
[54] N. Wilkins-Diehr, Special issue: science gateways—common community interfaces to grid resources, Concurrency and Comput.: Pract. and Exp. 19 (2007) 743–749.
[55] N. Wilkins-Diehr, D. Gannon, G. Klimeck, S. Oster, S. Pamidighantam, TeraGrid science gateways and their impact on science, IEEE Computer 41 (2008) 32–41.
[56] See http://nanoHUB.org. The nanoHUB.org science gateway focuses on the online simulation of nanoelectronics and has supported an annual user base that now exceeds 230 K, Over 11 K users have run over 360 K simulations in the past 12 months.
[57] G. Klimeck, M. McLennan, S. Brophy, G. Adams III, M. Lundstrom, nanoHUB.org: advancing education and research in nanotechnology, IEEE Comput. Eng. Sci. 10 (2008) 17–23.
[58] A. Strachan, G. Klimeck, M. Lundstrom, Cyber-enabled simulations in nanoscale science and engineering, Comput. Sci. Eng. 12 (2010) 12–17.
[59] G. Klimeck, G. Adams III, K. Madhavan, N. Denny, M. Zentner, S. Shivarajapura, L. Zentner, D. Beaudoin, Social networks of researchers and educators on nanohub.org, in: Proc. of IEEE/ACM International Symposium on Cluster, Cloud and Grid Computing, CCGrid, 2011.
[60] D. Nam, J.H. Lee, S. Hwang, Y.-K. Suh, B. Kim, Research process support with organizational flow in e-science, in: Proc. of the IEEE/ACIS International Conference on Computer and Information Science, 2008.
[61] J. Basney, M. Humphrey, V. Welch, The MyProxy online credential repository, Softw. Pract. Exp. 00 (2005) 1–17.
[62] V. Welch, F. Siebenlist, I. Foster, J. Bresnahan, K. Czajkowski, J. Gawor, C. Kesselman, S. Meder, L. Pearlman, S. Tuecke, Security for Grid services, in: Proceedings of the IEEE International Symposium on High Performance Distributed Computing, 2003.